Journal of Applied Physics

Design considerations for tailoring the thickness profile of transparent dielectric deposits by continuous-wave laser deposition

Cite as: J. Appl. Phys. **113**, 013108 (2013); https://doi.org/10.1063/1.4773332
Submitted: 15 October 2012 . Accepted: 10 December 2012 . Published Online: 07 January 2013

J. M. González-Leal, and J. Valverde

HIDEN ANALYTICAL Instruments for Advanced Science
- Knowledge,
- Experience,
- Expertise

Click to view our product catalogue

Contact Hiden Analytical for further details:
W www.HidenAnalytical.com
E info@hiden.co.uk

- dynamic measurement of reaction gas streams
- catalysis and thermal analysis
- molecular beam studies
- dissolved species probes
- fermentation, environmental and ecological studies

- UHV TPD
- SIMS
- end point detection in ion beam etch
- elemental imaging - surface mapping

- plasma source characterization
- etch and deposition process reaction kinetic studies
- analysis of neutral and radical species

- partial pressure measurement and control of process gases
- reactive sputter process control
- vacuum diagnostics
- vacuum coating process monitoring

© 2013 American Institute of Physics.

JOURNAL OF APPLIED PHYSICS 113, 013108 (2013)

Design considerations for tailoring the thickness profile of transparent dielectric deposits by continuous-wave laser deposition

J. M. González-Leal[a)] and J. Valverde
Department of Condensed Matter Physics, Faculty of Sciences, University of Cadiz, 11.510 Puerto Real (Cadiz), Spain

(Received 15 October 2012; accepted 10 December 2012; published online 7 January 2013)

The distribution of a transparent dielectric material deposited onto a planar substrate by a continuous-wave laser is studied concerning the dependence on the light-intensity distribution. Theory is derived to model the thickness profile of the condensed material, with the aim of supporting the fabrication of free-from optics. Experiments have been performed to test the theory on the basis of an infrared-transmitting chalcogenide glass. © *2013 American Institute of Physics*. [http://dx.doi.org/10.1063/1.4773332]

I. INTRODUCTION

Laser sources have shown their usefulness for material processing and fabrication since its invention in 1960. The deposition of a number of materials onto different substrates has been achieved and intensive research regarding targets, deposition geometry, and physical mechanism involved in the process has been under development since then.[1–3] Most of the laser deposition techniques have traditionally been addressed towards planar technologies and based upon the use of pulsed laser sources, giving raise to the well-known pulsed laser deposition (PLD) techniques.[1,2]

Alternatively, the use of laser deposition techniques for the fabrication of refractive optical elements by tailoring the thickness profile of dielectric deposits onto transparent substrates is being explored as a promising procedure for both reducing fabrication costs and designing complex optical elements (including freeform and hybrids).[4–6] In the course of the present research, results have been reported by the authors for the fabrication of axicon-like lenses made from infrared (IR) transparent amorphous semiconducting targets using a cw laser source.[5,6] Information about the optical performance of these axicon-like lenses, as well as the analysis of the light propagation in terms of the stationary-phase approximation, can be found in Refs. 4–6.

The analysis of the deposit thickness profiles was performed in a previous work[6] from the fitting of an analytical function corresponding to an evaporation point-source to the thickness records measured by a stylus-based profilometer. Such a simplification was found to be relevant for the aims of testing the reproducibility of the deposition process and the distinct influence of intensity and time which follows a non-reciprocity law, depending on the laser power used. The aim of the present paper is to go further in the analysis of the thickness profiles by considering an extended evaporation source in better agreement with the experiments. Fabrication parameters will be derived from the integration of the point-source evaporation function over the real irradiated domain on the target material.

The paper is organized as follows. In Sec. II, we present the theory for the material evaporation from a target and the distribution of the condensate onto a planar substrate, when a point evaporation source is considered. Both the cases of effusion and non-effusion process are considered. We will extend the theory to the case of an arbitrary extended evaporation source. In this a case, we will consider the target is irradiated by an arbitrary light intensity distribution supplied by a cw laser source and we derive the material thickness profile. We describe the experimental setup for sample preparation in Sec. III, as well as the instrumentation used for both optical and thickness-profile measurements. Results are presented in Sec. IV and discussion is developed in Sec. V. Some conclusions are remarked in Sec. VI.

II. THEORY

Figure 1 sketches the geometrical configuration for the evaporation of a target material whose vapour will be condensate onto a near planar substrate. We will assume that at a given differential of target area, dA_v, the material is ejected at a mass evaporation rate $\Gamma = \Gamma(\varphi, \theta)$, which, in general, depend on both polar angle, θ, and azimuthal angle, φ, through the differential of solid angle

$$d\omega = \sin\theta \, d\theta \, d\varphi. \tag{1}$$

Due to the rotational symmetry of the problem with respect to azimuthal angle φ, the mass evaporation rate dependence with this angle is assumed to vanish and therefore $\Gamma = \Gamma(\theta)$. The mass flux evaporated into a solid angle $d\omega$ about an exit polar angle of θ can then be expressed as[7]

$$d^3 m_v = \Gamma(\theta)\cos(\theta)\frac{d\omega}{C} dA_v d\tau, \tag{2}$$

where $d\tau$ is a differential of time and C is a normalization constant. In the next, we will distinguish two cases according to $\Gamma(\theta)$.

[a)]Author to whom correspondence should be addressed. Electronic mail: juanmaria.gonzalez@uca.es. Telephone: +34-956-016569. Fax: +34-956-016288.

 © 2013 American Institute of Physics

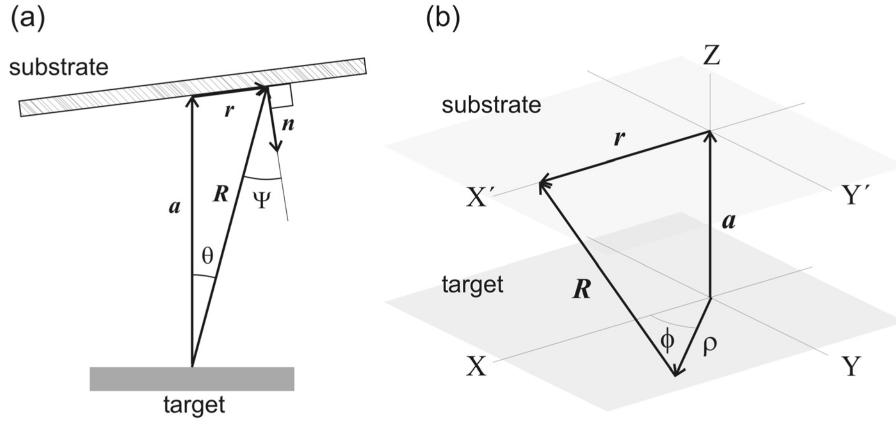

FIG. 1. 2D sketch of an arbitrary geometrical configuration of the target material and a planar substrate showing the distances and angles being relevant for the formulation developed in the manuscript (a). 3D sketch for the case of the target and substrate being parallel and an extended evaporation source (b).

A. Effusion process

Under effusion assumption, the dependence of the mass evaporation rate with respect to the polar exit angle, θ, can be removed and $\Gamma(\theta) = \Gamma$ (constant rate in all directions). In this case, Eq. (2) can be written as

$$d^3 m_e = \Gamma \cos(\theta) \frac{d\omega}{C} dA_v \, d\tau. \tag{3}$$

Note that $\int_\Omega \cos(\theta)\, d\omega = \int_0^{2\pi} \int_0^{\frac{\pi}{2}} \cos(\theta)\sin(\theta)\, d\theta\, d\varphi = \pi$ by substitution of Eq. (1). Therefore, the normalization constant would be $C = \pi$. Further integration on evaporation time and source area provides the differential of mass evaporated per differential of solid angle as

$$dm_e = \int_{A_v} \int_0^\tau d^3 m_e = \int_{A_v} \int_0^\tau \Gamma \cos(\theta) \frac{d\omega}{\pi} dA_v \, d\tau$$
$$= \cos(\theta) \frac{d\omega}{\pi} \int_{A_v} \int_0^\tau \Gamma \, dA_v \, d\tau. \tag{4}$$

The total mass of evaporated material in the effusion case can be written as

$$M = \int_{A_v} \int_0^\tau \Gamma \, dA_v \, d\tau, \tag{5}$$

which allows us rewriting Eq. (4) for a final expression of the differential of evaporated mass

$$dm_e = M \cos(\theta) \frac{d\omega}{\pi}. \tag{6}$$

Equation (6) represents the well-known *cosine law of emission* for effusion process. Following Knudsen[7,8] it can be easily verified that this law reflects the effective deposition of a perfect uniform coating inside a spherical glass jar. For a planar substrate as sketched in Fig. 1(a), we can obtain the specific thickness profile of the deposit using the conservation of mass law between the evaporated mass of the target and condensed mass onto the substrate, dm_c, as

$$dm_e = dm_c \Rightarrow M \cos(\theta) \frac{d\omega}{\pi} = dA_c \, t_e \, \rho_c, \tag{7}$$

where ρ_c is the mass density of the condensed material, t_e is the thickness of the resulting profile, and dA_c represents a differential of area of condensed material which can be related to the projection of the solid angle $d\omega$ onto the substrate plane using the definition of the differential of solid angle (see Eq. (1) and Fig. 1)

$$d\omega = \sin\theta \, d\theta \, d\varphi = \frac{\mathbf{R} \cdot \mathbf{n}}{R^3} dA_c, \tag{8}$$

where $\mathbf{R}$ is the position vector onto the substrate of the differential of area dA_c and $\mathbf{n}$ is the unit normal vector to such surface at this point. Introducing Eq. (8) into Eq. (7), substituting $\mathbf{R} \cdot \mathbf{n} = R\cos(\psi)$, and solving for the differential of thickness profile we obtain

$$t_e(r) = \frac{M}{\pi \rho_c} \frac{\cos^2\theta}{R^2} = \frac{M}{\pi \rho_c} \frac{1}{(1 + (r/a)^2)^2} = \frac{t_0}{(1 + (r/a)^2)^2} \tag{9}$$

for the case of target and substrate parallel, where the geometric relations $R = (a^2 + r^2)^{1/2}$ and $\cos(\theta) = \cos(\Psi) = a/R = a/(a^2 + r^2)^{1/2}$ have been used, with a standing for the distance between the target and substrate (see Fig. 2), and $t_0 = \frac{M}{\pi \rho_c}$ is the top thickness at $r = 0$. Note the dependence of the profile with r, the position on the planar substrate with respect to the axis of symmetry, as opposed to case of the spherical glass jar mentioned above where the thickness is constant.

B. Non-effusion process

When we separate from the ideal effusion case, the assumption of constant rate of mass ejection in all directions does not hold anymore. In such a case, we have to go back to

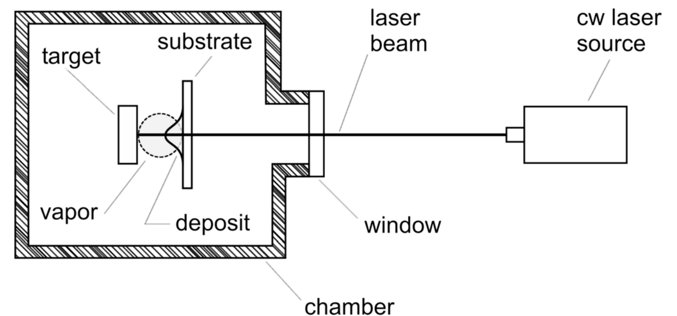

FIG. 2. Cross-section of the experimental setup used for the deposition in vacuum of a target material onto a planar substrate using a cw laser.

the original Eq. (2). We will assume a rate of mass of the form $\Gamma(\theta) = \Gamma\cos^p(\theta)$ and rewrite Eq. (2) as follows[8]

$$d^3m_{n-e} = \Gamma\cos^p(\theta)\cos(\theta)\frac{d\omega}{C}\, dA_v\, d\tau. \quad (10)$$

Taking into account that

$$\int_\Omega \cos^p(\theta)\cos(\theta)\, d\omega = \int_0^{2\pi}\int_0^{\frac{\pi}{2}} \cos^{p+1}(\theta)\sin(\theta)\, d\theta\, d\varphi = \frac{2\pi}{p+2}, \quad (11)$$

we can rewrite Eq. (10) as

$$\begin{aligned} d^3m_{n-e} &= \Gamma\cos^n(\theta)\frac{d\omega}{2\pi}(n+1)\, dA_v\, d\tau \Rightarrow dm_{n-e} \\ &= \cos^n(\theta)\frac{d\omega}{2\pi}(n+1)\int_{A_v}\int_0^\tau \Gamma\, dA_v\, d\tau \\ dm_{n-e} &= M\cos^n(\theta)\frac{d\omega}{2\pi}(n+1), \end{aligned} \quad (12)$$

where $n = p+1$ and the value of $p > 0$ gives account for the degree of departure from the effusion model mentioned above. Values of n in the range of 3–17 have been reported in the case of PLD processes.[1,2,9] On the other hand, considering Eq. (8) and the geometric relations introduced earlier for target and substrate parallel, the thickness profile of a deposit in the case of non-effusion process can be written as

$$t_{n-e}(r) = \frac{dm_{n-e}}{dA_c} = \frac{M(q-1)}{\pi\rho_c a^2}\frac{1}{(1+(r/a)^2)^q} = \frac{t_0}{(1+(r/a)^2)^q}, \quad (13)$$

where $t_0 = \frac{M(q-1)}{\pi\rho_c a^2}$ is the top thickness at $r=0$ and $q = (n+3)/2$. In some cases, as the one reported for PLD chalcogenide samples,[9] a linear combination of Eq. (13) has been used to fit the deposit profiles

$$t_{PLD}(r) = \sum_i \beta_i \frac{t_{0i}}{(1+(r/a)^2)^{q_i}}, \sum_i \beta_i = 1. \quad (14)$$

C. Non-effusion over extended evaporation source

The cases above consider point evaporation sources. Equation (12) can be modified to account for the case of an evaporation source extended over the target surface as illustrated in Fig. 1(b). In such a case, at point ρ over the target material, a differential of total mass, dM, is ejected to deposit a differential of thickness profile, $dt(r)$.

In this case, the following trigonometric relations $R^2 = a^2 + r^2 + \rho^2 - 2r\rho\cos(\phi) = a^2 + (r-\rho)^2 + 4r\rho\sin^2(\phi/2)$ must be used. We proceed as in the previous case, matching the evaporated and condensed differential of mass as

$$\left.\begin{aligned} d^2m &= dM\cos^n(\theta)\frac{d\omega}{2\pi}(n+1) \\ d^2m_c &= dA_c\, dt(r)\,\rho_c \end{aligned}\right\}. \quad (15)$$

After some manipulations, the differential of thickness profile can be expressed as

$$dt(r) = (q-1)\frac{dM}{\pi a^2\rho_c}\frac{1}{\left(1+\frac{(r-\rho)^2+4r\rho\sin^2(\phi/2)}{a^2}\right)^q}. \quad (16)$$

Bearing in mind that we are interested in using a laser beam as heat supply to produce the evaporation, we will assume that the differential of evaporated mass dM depends in linear form on the light intensity distribution over the target surface, $I(\rho)$,

$$d^2M = \eta\frac{I(\rho)}{L_{re}}\, dA_v\, d\tau, \quad (17)$$

where L_{re} stands for the material removal energy, and factor η stands for the fraction of the laser energy being absorbed by the target which can be modelled taking into account the reflectance corresponding to the optical elements between the laser source and the target, as well as the reflectance at the target surface, R_i, i.e.,

$$\eta = \prod_i (1-R_i). \quad (18)$$

This part of the model needs the explanation that follows, in order to support Eq. (17), namely: In a previous work, it was reported that at moderate intensities of the order of 10 W/cm^2 and in the case of IR-transmitting As-S glasses, a linear dependence between the evaporated mass and light intensity was measured when a cw laser at 532 nm wavelength is used for evaporation.[9] Measurements were taken by monitoring the reflectance of the sample while being deposited. A low-intensity He-Ne laser was used for monitoring. In all cases, significant delays were observed before evaporation occurs and a non-linear transient period was also measured before reaching the linear steady state. It is worth mentioning that this transient state was longer at intensities below 10 W/cm^2 and almost insignificant at intensities above 10 W/cm^2. We will focus our model to the latter case, and it will be introduced in the theory in the form of a threshold time τ_0 that models the energy devoted to reach the vaporization temperature. In this way, we can integrate Eq. (17), resulting

$$dM = \eta\frac{dQ_t}{L_{re}} = \int_{\tau_0}^{\tau}\eta\frac{I(\rho)}{L_{re}}\, dA_v\, d\tau = \eta\frac{I(\rho)}{L_{re}}(\tau-\tau_0)dA_v. \quad (19)$$

Thus, Eq. (16) can be rewritten as follows to model the thickness profile of the deposit:

$$\begin{aligned} t(r) &= \int_{A_v} dt = \frac{q-1}{\pi a^2\rho_c L_{re}}\eta(\tau-\tau_0) \\ &\times \left\{\int_{A_v}\frac{I(\rho)}{\left(1+\frac{(r-\rho)^2+4r\rho\sin^2(\phi/2)}{a^2}\right)^q}dA_v\right\}. \end{aligned} \quad (20)$$

Equation (20) could be used to solve the inverse problem of the design of axisymmetric complex optical elements, by defining the geometrical configuration of the setup, a and ρ_0,

the target characteristics, ρ_c, L_{re}, η and τ_0, the light intensity distribution $I(\rho)$ on the target, the exposure time τ, and the emission parameter q, and using a fitting procedure for the desired optical element shape.

D. Gaussian laser irradiation

Just to finish this theoretical section, we will consider a collimated Gaussian beam with beam radius σ, top intensity I_0 and total power P, as the heat supply for target evaporation. This corresponds to the results reported in the present work to support the theory. In such a case, the light intensity distribution can be modelled as

$$I(\rho) = I_0\,\mathrm{Exp}\left(\frac{-2\rho^2}{\sigma^2}\right) = \frac{2P}{\pi\,\sigma^2}\mathrm{Exp}\left(\frac{-2\rho^2}{\sigma^2}\right). \tag{21}$$

Introducing Eq. (21) into Eq. (19), the differential of total mass can be rewritten as

$$dM = \eta\frac{2P}{\pi\,\sigma^2 L_{re}}(\tau-\tau_0)\,\mathrm{Exp}\left(\frac{-2\rho^2}{\sigma^2}\right)dA_v. \tag{22}$$

Taking into account the radial symmetry of the problem, see Fig. 1(b), the infinitesimal area dA_v on the target surface plane can be defined in polar coordinates as

$$dA_v = \rho\,d\rho\,d\phi. \tag{23}$$

Inserting Eqs. (21) and (23) into Eq. (20), the thickness profile can be derived by solving the following integral over the evaporation source area

$$\begin{aligned} t(r;L_{re},q,\rho_0) &= \int_{A_v} dt = \frac{q-1}{\pi^2\sigma^2a^2\rho_c L_{re}}\eta P(\tau-\tau_0)\int_0^{\rho_0}\int_0^{2\pi}\frac{\exp(-2\rho^2/\sigma^2)}{\left(1+\frac{(r-\rho)^2+4r\,\rho\sin^2(\phi/2)}{a^2}\right)^q}\rho\,d\phi\,d\rho \\ &= A\int_0^{\rho_0}\int_0^{2\pi}\frac{\exp(-2\rho^2/\sigma^2)}{\left(1+\frac{(r-\rho)^2+4r\,\rho\sin^2(\phi/2)}{a^2}\right)^q}\rho\,d\phi\,d\rho, \end{aligned} \tag{24}$$

where ρ_0 is the mean radius of the area affected by the laser beam, which can be measured from the laser marks made on the targets, and

$$A = A(\tau) = \frac{q-1}{\pi^2\sigma^2a^2\rho_c L_{re}}\eta P(\tau-\tau_0). \tag{25}$$

A least-squares best fitting algorithm can be implemented from Eq. (24), in order to analyse the experimental thickness records, $t_{\exp}(r)$, measured with the stylus-based profilometer, via the function

$$f = \sum_i \left(t_{\exp}(r_i) - t(r_i;A,q)\right)^2, \tag{26}$$

to be minimised through the conditions

$$\frac{\partial f}{\partial A} = \frac{\partial f}{\partial q} = 0. \tag{27}$$

III. EXPERIMENTAL

Samples reported here have been obtained using a cw Nd:YVO_4 laser source emitting laser radiation at 532 nm (Coherent, model Verdi 6 V), and $As_{20}S_{80}$ glass alloy as starting material. This chalcogenide alloy was originally synthesized in bulk form, from their 5 N-purity constituents, by conventional melt-quenching in air. Target materials were made in tablet form, 13 mm in diameter and about 1 mm in thickness, from this bulk alloy. Tablets were all synthesized from the glass powder by pressing 125 mg of the starting material at 10 tons for 5 min, with the help of a pneumatic press. Depositions were performed according to the setup illustrated in Fig. 1 onto 5 mm thick, 1-in. radius, $\lambda/10$ planar (at $\lambda = 633$ nm), transparent crystalline (0001) quartz substrates in 10^{-5} Torr vacuum. Substrates were placed at 1.60 ± 0.05 mm minimum distance from the target, as measured with a calliper. The thickness profiles of the deposits as well as the laser marks on the targets were measured with a stylus-based profilometer (Veeco, model Dektak 150D) using a 0.7 μm radius tip. The optical transmittance the chamber window, T_w, and deposited samples, T_s, were measured at 532 nm wavelength by means of a double-beam ratio-recording spectrophotometer (Perkin Elmer, model Lambda-19). Specular reflectance of the targets, R_t, was also measured at 532 nm wavelength with the same spectrophotometer. The optical transmittance of the target was also measured to check its opacity. All measurements have been performed at ambient temperature.

IV. RESULTS

Figure 3 shows the optical transmission spectra corresponding to the quartz window of the chamber, a representative deposit onto a transparent quartz substrate and a representative target. Specular reflection spectrum of the target has also been included in this figure. The effective laser energy being absorbed by the target at 532 nm wavelength

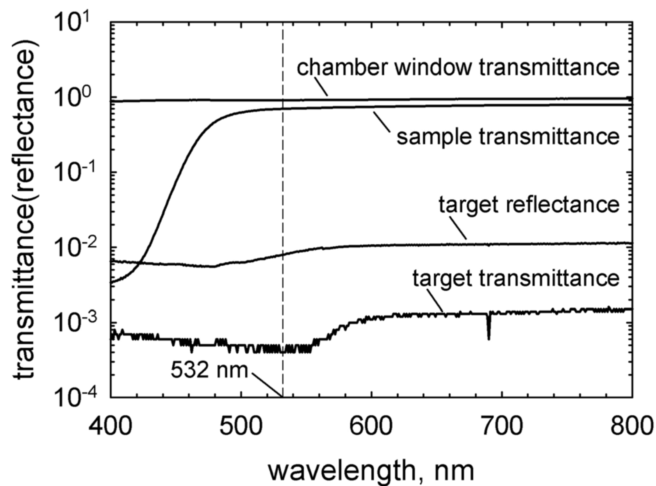

FIG. 3. Optical transmission of to the chamber window, sample deposited onto quartz substrate and the target. Also, reflection spectrum of the target.

has been determined from these measurements, giving a value for $\eta = T_w \times T_s \times (1 - R_t) = 0.91 \times 0.75 \times (1 - 0.08) = 0.586$. Optical transmittance of target was measured to be 4×10^{-4} showing that the laser light is most absorbed by the target.

Figure 4(a) shows the picture of a representative target after a set of irradiations with a collimated 1.25 mm radius, 0.58 W power, Gaussian laser beam ($I_0 = 11.8\ \mathrm{W/cm^2}$), and

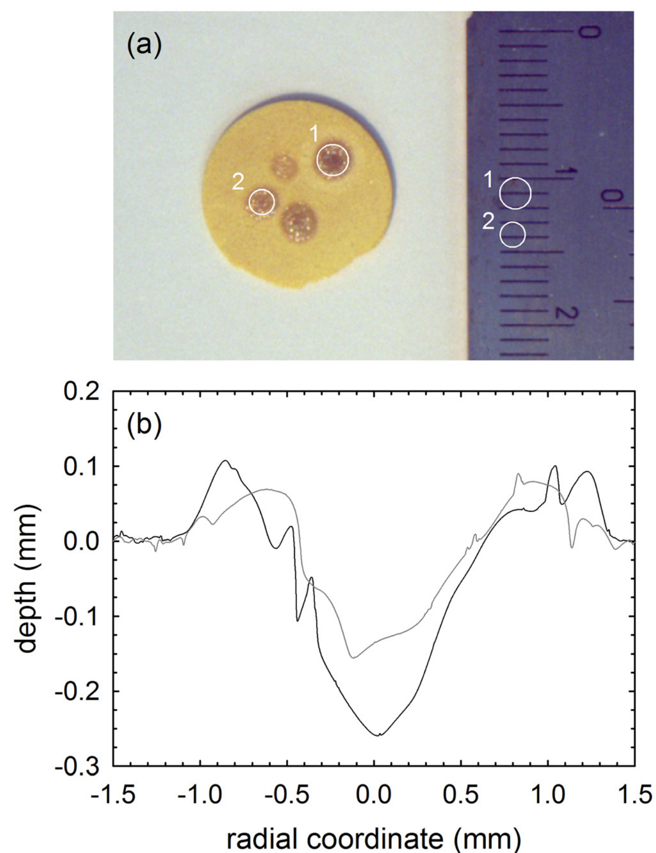

FIG. 4. Picture of a representative target material showing several marks made by a cw laser at 532 nm wavelength, after evaporation in vacuum according to the setup illustrated in Fig. 2. Mark sizes are estimated by comparison with a calliper (a). More precise measurements of the mark diameters and depths were made using a mechanical profilometer (b).

different exposure times. The area of the evaporation source has been marked to estimate the values for ρ_0 used in Eq. (24). For more precise values, the cross-sections of the laser marks were also measured by the profilometer and they are plotted in Fig. 4(b). It is worth mentioning that laser marks on the target surface evidence both that no ablation occurs and evaporation proceeds after fusion. It has been checked that when the evaporation starts at constant-rate material emission, the laser-mark radius, ρ_0, is about 5 mm in all cases.

Figure 5(a) shows the thickness profile along with its corresponding best fitting curve obtained from Eq. (24), for a representative deposit fabricated at $I_0 = 11.8\ \mathrm{W/cm^2}$ intensity and 12 s exposure time. The contour plot of the thickness profile of this deposit is illustrated in Fig. 5(b). The value of the eccentricity has been measured to be 0.27 from this contour plot. The surface roughness of the samples has been analyzed from the corresponding thickness profiles. A value of 0.02 μm (root mean square) has typically been obtained for the samples studied in this work.

Values of the fitting parameter A for samples prepared at $I_0 = 6.1$, 9.0, 10.2, 11.8, 14.7, 17.5, and 20.4 W/cm^2 are shown in Fig. 6 as a function of the exposure time, according to Eq. (25), along with the corresponding least-squared straight lines. Evaporation delays τ_0 calculated from these

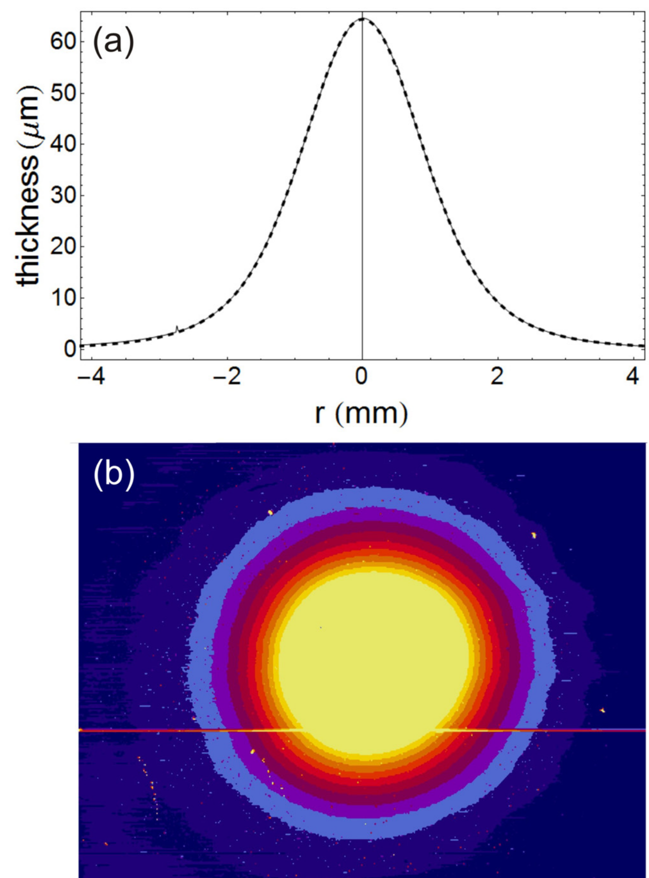

FIG. 5. Thickness profile measured by the mechanical profilometer of a representative deposit made at 11.8 W/cm^2 intensity and 12 s exposure time, along with the theoretical curve obtained by the best-fitting procedure based on Eq. (24) (a). Contour plot of the thickness profile to measure the eccentricity of this deposit (b). The line appearing in this figure is an artifact due to the dragging of a particulate by the stylus over the sample surface.

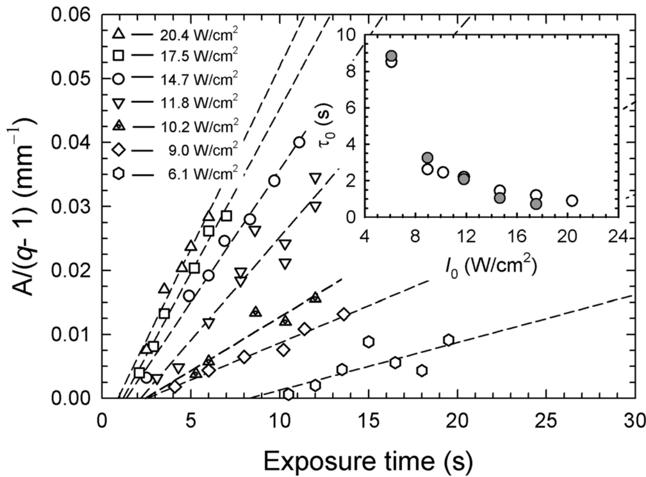

FIG. 6. Plot the values for the factor $A/(q-1)$ obtained from the best-fitting curves to the thickness profiles of samples prepared at different laser intensities, as a function of the exposure time. Evaporation delays τ_0 calculated from the least-squared straight lines for these data are plotted in the inset against laser intensity. Values of τ_0 derived from the results reported in Ref. 9 are also plotted in the inset for comparison.

least-squared straight lines for these data are plotted in the inset against laser intensity. Values of τ_0 derived from the results reported in Ref. 9 are also plotted for comparison. The values of the slope parameters obtained from the least-squared straight-line equation of Fig. 6, $A/(q-1) = b_0 + b_1 \tau$, have been used to calculate the removal energy, L_{re}, in Fig. 7 by also least-squared fitting of b_1 data vs I_0. Values of b_1 at lower intensities 6.1, 9.0, and 10.2 W/cm^2 have been discarded in the fit of Fig. 7, as the material emission rate departs in those cases from the model considered in Eq. (19).

V. DISCUSSION

First to highlight is the significant linear dependence observed in Fig. 6 between the values of the A parameter for different laser intensities and the exposure time τ, according to Eq. (25). Also, values of the delay τ_0 calculated from least-squared straight line to these data are consistent with those directly measured during the deposition process.[10] These results sound the practical usefulness of the linear model used for the energy balance, although the model does not account accurately for either the heat transport or phase changes occurring in the target. It should be noted that the effect of these processes is expected to be more relevant in laser evaporations at low intensities. This was observed in Ref. 10 where the material emission accelerating stage was more significant and it took more time to reach the evaporation steady stage. However, for moderate laser intensities, namely of the order of 10 W/cm^2, such evaporation accelerating stage is not that significant and the process early occurs at constant rate in similar way as the model considered in Eq. (19), i.e., material emission = 0, if $0 < \tau \leq \tau_0$ and material emission = $\alpha(\tau - \tau_0)$, if $\tau > \tau_0$, with α = constant.

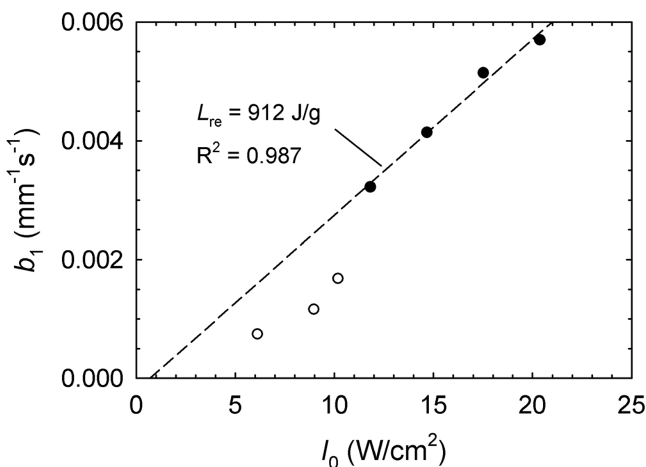

FIG. 7. Determination of the removal energy parameter L_{re} from the slopes, b_1, of the least-squared straight-line equations of Fig. (6). The value of the correlation coefficient, R^2, is shown in the figure. Values at lower intensities 6.1, 9.0, and 10.2 W/cm^2 have been discarded in the fit as the material emission rate departs in those cases from the model considered in Eq. (19).

As a test of the results, the value for the removal energy L_{re} has been derived from the slope of the least-squared straight-line equations of Fig. 6. A value of L_{re} = 912 J/g has been derived, considering a value for the mass density ρ_c = 2.585 g/cm^3 for the $As_{20}S_{80}$ glass alloy used.[11] It is worth mentioning that stoichiometry holds for this alloy in the condensate material, as it has been reported in previous works.[12] This value would account for both the heat of fusion and the heat of vaporization of the $As_{20}S_{80}$ alloy used, besides other phenomena specifically occurring in the evaporation process which will be discussed later. Unfortunately, we did not manage to find values of these thermodynamic quantities in the literature for this particular alloy in order to enrich the discussion. Nonetheless, the result can be compared with the heat of vaporization and fusion reported for the stoichiometric $As_{40}S_{60}$ alloy of 903 J/g (Ref. 13) and 131 J/g,[14] respectively, and the heat of vaporization and fusion for the monoclinic sulphur allotrope of 326 J/g and 50.1 J/g, respectively.[15]

Bearing in mind that we are dealing with a sulfur-rich $As_{20}S_{80}$ alloy, our value of 912 J/g would be consistent with those values. Nevertheless, it should be taken into account that this value also includes the energy needed to sequentially increase the temperature up to the fusion and vaporization points, and it would be affected by the fact of using a pressed-powder target. On the other hand, a relief is observed along the border of the laser mark on the target, as illustrated in Fig. 4. This could be related with the well-known volume increase on melting of 8.5% occurring in monoclinic sulphur.[15] The occurrence of this effect would have an effect in the increase of the removal energy L_{re}, and vapour condensation at these borders and in turn to material re-evaporation could have place during the process.

To the respect of the border relief, values of the q parameter standing for the material-emission directionality have been found to be larger, about 2.4 for the highest doses of 8 J used in the present study, in comparison with the values about 2 for the lower doses: a gradual increase is observed in the q values as a function of doses within the certainty of our best-fitting procedure. This seems to us consistent with the occurrence of this relief along the border of the laser marks as it obstacles having effect on the directionality of the vapour.

It is also observed in Fig. 4 that the depth of the laser marks increases with the supplied energy with a maximum value of 0.25 mm for the highest laser energy of 8 J. This would have an effect on the value of the target-substrate gap parameter, a, and it could be introduced in the theory in the form of a function of the exposure time, i.e., $a = a(\tau)$. In the same way, ρ_0 should also be considered in similar form $\rho_0 = \rho_0(\tau)$. The vanishing of these time-dependent functions into the model could be seen as a weakness. Nevertheless, our results seem to indicate that the influence of these time-dependent functions is not strong, at least at the doses used in the present work, and the hole evolving in the target could be playing in similar way of a Knudsen cell, in such a fashion that the thermalization hypothesis of the effusion process is hold in some resemble in the cw laser deposition of the present samples.

This weakness of the model, or the cw laser-deposition technique, depending on the point of view, could be superseded if a low-viscosity target is used instead (or a liquid provided evaporation is controlled). In such a case, the target-substrate gap would hold constant, and ρ_0 would be purely related with the laser beam. This could be realized by a heater installed in the chamber to increase the temperature until reaching the glass transition temperature of the target material. Expected drawback in this case would be related to the increase of the target reflectance in comparison with the use of the pressed-powder tablet used here. Such a drawback was observed in the experiments performed using a planar piece of $As_{20}S_{80}$ bulk as the target material (without heat supply). A notable reduction in the deposition efficiency was measured as a consequence of the higher surface reflectance of the target, as well as the larger heat diffusion coefficient. Laser marks with border reliefs similar to the ones reported here for pressed-powder tablets were also observed.

Finally, it is worth mentioning that an important limitation for free-form optics fabrication by the deposition technique described here would be the minimum resolution that can be reached in the surface relief details. As it has been described above, the technique does not produce a point-to-point transfer of material from the target to the substrate, but a material distribution over the substrate with a FWHM comparable to the target-substrate gap in the case of the effusion process. Higher directionality could be reached if pulsed lasers are used instead, with distribution of the ablated material being sharper. In such a case, the resolution of the surface relief details could be improved. Nevertheless, other technical drawbacks concerning stoichiometry of the condensate material could appear in these cases.

VI. CONCLUSIONS

Theory has been developed to model the thickness profile of transparent dielectric deposits made by cw laser evaporation in off-axis configuration. Theory has been compared with the experimental thickness profiles produced using a 532 nm wavelength cw Gaussian beam at different intensities and doses. An $As_{20}S_{80}$ glass alloy has been used as the target. This material being of interest as it is IR transparent. Comparison has been performed through a least-squared best fitting procedure with two free parameters. Although excellent agreement has been found between the mathematical model and the experimental results, improvements could be made to increase the precision of the cw laser deposition process for the fabrication of free-form optics.

ACKNOWLEDGMENTS

This work has been partly supported by the Spanish Ministry of Education and Science through the National Physics I+D+i Programme (Spain), under the FIS2008-00260 project, and by the Regional Ministry of Innovation, Science and Enterprise of Andalusia, through the Excellence Research Programme, under the FQM-4239 project. J.V. wants to thank Regional Ministry for financial support.

[1] D. B. Chrisey and G. K. Hubler, *Pulsed Laser Deposition of Thin Films* (Wiley-Interscience, New York, 1994).
[2] R. Eason, *Pulsed Laser Deposition of Thin Films: Applications-Led Growth of Functional Materials* (Wiley-Interscience, NJ, 2007).
[3] D. R. Olander, Pure Appl. Chem. **62**, 123 (1990).
[4] J. M. González-Leal and J. A. Angel, Opt. Lett. **32**, 2384 (2007).
[5] J. M. González-Leal, Opt. Express **15**, 5451 (2007).
[6] J. M. González-Leal, J. A. Ángel, L. Rubio-Peña, J. Valverde, and A. Gámez, Thin Solid Films **518**, 5530 (2010).
[7] L. I. Maissel and R. Glang, *Handbook of Thin Film Technology* (McGraw-Hill, New York, 1983).
[8] K. L. Saenger, in *Pulsed Laser Deposition of Thin Films*, edited by D. B. Chrisey and G. K. Hubler (Kluwer, New York, 1994).
[9] M. Pavlista, M. Hrdlicka, P. Nemec, J. Prikryl, and M. Frumar, Appl. Phys A **93**, 617 (2008).
[10] J. M. González-Leal, J. A. Ángel, L. Rubio-Peña, and J. Valverde, Thin Solid Films **520**, 5512 (2012).
[11] Z. U. Borisova, *Glassy Semiconductors* (Plenum, New York, 1981).
[12] J. M. González-Leal, A. J. Gámez, J. A. Ángel, and R. Jiménez Garay, J. Non-Cryst. Solids **355**, 1989 (2009).
[13] A. V. Rode, A. Zakery, M. Samoc, R. B. Charters, E. G. Gamaly, and B. Luther-Davies, Appl. Surf. Sci. **197–198**, 481 (2002).
[14] P. Espeau, J. Ll. Tamarit, M. Barrio, D. Ó. López, M. A. Perrin, H. Allouchi, and R. Céolin, Chem. Mater. **18**, 3821 (2006).
[15] J. L. Sudworth and A. R. Tilley, *The Sodium Sulfur Battery* (Chapman and Hall, New York, 1985).